



Contents lists available at ScienceDirect

# Spectrochimica Acta Part A: Molecular and Biomolecular Spectroscopy

journal homepage: [www.elsevier.com/locate/saa](http://www.elsevier.com/locate/saa)

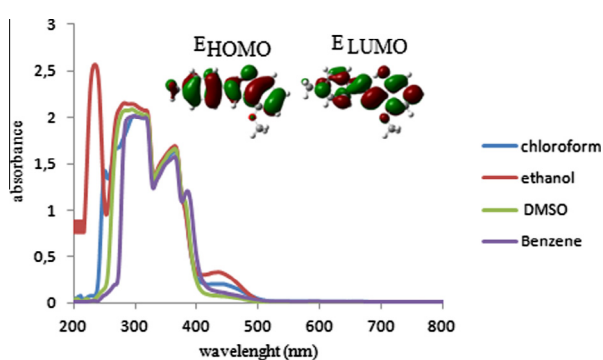
## Experimental (X-ray, FT-IR and UV–vis spectra) and theoretical methods (DFT study) of (E)-3-methoxy-2-[(p-tolylimino)methyl]phenol

Zeynep Demircioğlu<sup>a,\*</sup>, Çiğdem Albayrak<sup>b</sup>, Orhan Büyükgüngör<sup>a</sup><sup>a</sup> Department of Physics, Faculty of Arts and Sciences, Ondokuz Mayıs University, TR-55139 Kurupelit-Samsun, Turkey<sup>b</sup> Department of Chemistry, Faculty of Arts and Science, Sinop University, TR-57000 Sinop, Turkey

### HIGHLIGHTS

- Experimental (X-ray, FT-IR and UV–vis spectra) methods and theoretical methods (DFT study) were investigated.
- Nonlinear optical properties (NLO) and natural bond orbital (NBO) analysis were analyzed.
- Mulliken population method and natural population analysis (NPA) were calculated.

### GRAPHICAL ABSTRACT



### ARTICLE INFO

#### Article history:

Received 11 December 2013

Received in revised form 24 February 2014

Accepted 25 February 2014

Available online 12 March 2014

#### Keywords:

Schiff bases

Natural population analysis (NPA)

Density functional theory (DFT)

Molecular electrostatic potential (MEP)

Nonlinear optical properties (NLO)

Natural bond analysis (NBO)

### ABSTRACT

A suitable single crystal of (E)-3-methoxy-2-[(p-tolylimino)methyl]phenol, formulated as  $C_{15}H_{15}N_1O_2$ , reveals that the structure is adopted to its E configuration about the azomethine  $C=N$  double bond. The compound adopts a enol–imine tautomeric form with a strong intramolecular  $O-H\cdots N$  hydrogen bond. The single crystal X-ray diffraction analysis at 296 K crystallizes in the monoclinic space group  $P2_1/c$  with  $a = 13.4791(11)$  Å,  $b = 6.8251(3)$  Å,  $c = 18.3561(15)$  Å,  $\alpha = 90^\circ$ ,  $\beta = 129.296(5)^\circ$ ,  $\gamma = 90^\circ$  and  $Z = 4$ . Comprehensive theoretical and experimental structural studies on the molecule have been carried out by FT-IR and UV–vis spectrometry.

Optimized molecular structure and harmonic vibrational frequencies have been investigated by DFT/B3LYP method with 6-31G(d,p) basis set. Stability of the molecule, hyperconjugative interactions, charge delocalization and intramolecular hydrogen bond has been analyzed by using natural bond orbital (NBO) analysis.

Electronic structures were discussed by TD-DFT method and the relocation of the electron density were determined. The energetic behavior of the title compound has been examined in solvent media using polarizable continuum model (PCM). Molecular electrostatic potential (MEP), Mulliken population method and natural population analysis (NPA) have been studied. Nonlinear optical (NLO) properties were also investigated. In addition, frontier molecular orbitals analysis have been performed from the optimized geometry. An ionization potential ( $I$ ), electron affinity ( $A$ ), electrophilicity index ( $\omega$ ), chemical potential ( $\mu$ ), electronegativity ( $\chi$ ), hardness ( $\eta$ ), and softness ( $S$ ), have been investigated.

© 2014 Elsevier B.V. All rights reserved.

\* Corresponding author. Tel.: +90 362 312 1919.

E-mail address: [zeynep.kelesoglu@omu.edu.tr](mailto:zeynep.kelesoglu@omu.edu.tr) (Z. Demircioğlu).

## Introduction

Schiff bases are important in diverse fields of chemistry and biochemistry owing to their biological activity [1,2] and can be classified according to their photochromic or thermochromic properties [3,4]. From observations on some thermochromic and photochromic Schiff base compounds, it was proposed that molecules exhibiting thermochromism are planar, while those exhibiting photochromism are non-planar [5,6]. *o*-hydroxy schiff base ligands are of interest mainly because of the existence of typical hydrogen bonds and tautomerism between the O—H···N in phenol-imine and N—H···O in keto-amine forms and N<sup>+</sup>—H···O<sup>-</sup> in zwitterionic forms [7–9]. This compound undergoes tautomerism by proton transfer between the hydroxy O atom and the imine N atom, namely the enol-imine tautomer. In Schiff base compounds, the imine nitrogen can act as an inter- or intramolecular hydrogen-bond acceptor and the hydroxyl oxygen in salicylaldehyde derivatives can act as an intermolecular hydrogen-bond acceptor. Schiff bases non-linear properties have an importance for the design of various molecular electronic devices such as optical switches and optical data storage devices [10,11].

For Schiff bases, NLO studies provide the key functions of frequency shifting, optical modulation, optical switching, optical logic, and optical memory for the emerging technologies in areas such as telecommunications, signal processing, and optical interconnections.

The title molecule was determined by single crystal X-ray diffraction technique. In the present study, it is planned to have a joint experimental and theoretical investigation of FT-IR and UV-vis spectra. Electronic absorption spectra of the title compound were predicted by using time-dependent density functional theory (TD-DFT) [12–14] in the calculation of electronic excitation energies for gas and solution phases (different solvent media). The excitation energies, wavelengths and oscillator strengths were obtained at TD-DFT level at the optimized geometry. In addition to, it is also planned to illuminate theoretical determination of the optimized molecular geometries, HOMO–LUMO energy gap, MEP, NLO, Mulliken charges, NPA and NBO analysis of the title compound by using density functional theory (DFT) with B3LYP/6-31G(d,p) basis set. In addition, the ionization potential, electron affinity, electrophilicity index, chemical potential, electronegativity, hardness and softness are determined.

## Experimental and computational methods

### Synthesis

For the preparation of (E)-3-methoxy-2-[(*p*-tolylimino)methyl]phenol compound the mixture of 2-hydroxy-6-methoxybenzaldehyde (0.5 g, 3.3 mmol) in ethanol (20 ml) and 4-methylaniline (0.35 g, 3.3 mmol) in ethanol (20 ml) was stirred for 2 h under reflux. The crystals suitable for X-ray analysis were obtained from ethanol by slow evaporation (yield; %84, m.p.; 342–344 K).

### Instrumentation

The FT-IR spectrum of the title compound was recorded in the 4000–400 cm<sup>-1</sup> region with a Bruker Vertex 80V FT-IR spectrometer using KBr pellets. Absorption spectra were determined on Unicam UV-vis spectrometer.

### Crystal structure determination

The single-crystal X-ray data were collected on a STOE IPDS II image plate diffractometer at 296 K. Graphite-monochromated

Mo K $\alpha$  radiation ( $\lambda = 0.71073 \text{ \AA}$ ) and the  $\omega$ -scan technique were used. The structure was solved by direct methods using SHELXS-97 [15] and refined through the full-matrix least-squares method using SHELXL-97 [16], implemented in the WinGX [17] program suite. Non-hydrogen atoms were refined with anisotropic displacement parameters. All H atoms were located in a difference Fourier map and were refined isotropically. Data collection: Stoe X-AREA [17], cell refinement: Stoe X-AREA [17], data reduction: Stoe XRED [18]. The general-purpose crystallographic tool PLATON [19] and ORTEP-3 [17] was used for the structure analysis and presentation of the results. The structure was refined to  $R_{\text{int}} = 0.030$  with 2132 observed reflections using  $I > 2\sigma(I)$  threshold. Details of the data collection conditions and the parameters of the refinement process are given in Table 1.

### Computational details

The entire calculations conducted in the present work were performed at B3LYP levels included in the Gaussian 03 W package [20] program together with 6-31G(d,p) basis set function of the density functional theory (DFT) utilizing gradient geometry optimization [21]. Initial geometry generated from standard geometrical parameters was minimized without any constraint in the potential energy surface at Hartree–Fock level, adopting the standard 6-31G(d,p) basis set. We have utilized the gradient corrected density functional theory [22] with three parameter hybrid functional (B3) [23] for the exchange part and the Lee–Yang–Parr (LYP) correlation function [24], accepted as a cost effective approach for the computation of molecular structure, vibrational frequencies and energies of optimized structures. By combining the results of the Gaussview program [25] with symmetry considerations, vibrational frequency assignments were made with a high degree of accuracy.

The significant values for energy, bond lengths, bond angles and torsions were obtained by using B3LYP/6-31G(d,p) basis set. The optimized structural parameters were used in the vibrational frequency calculations at the DFT levels to characterize all stationary points as minima. At the optimized structure of the examined species, no imaginary frequency modes were obtained proving that a true minimum on the potential energy surface was found. We have scaled the vibration frequency numbers with standard scaling factor 0.9627 to neglect of vibrational anharmonicity.

**Table 1**

Crystal data and structure refinement parameters for the title compound.

Chemical formula	C <sub>15</sub> H <sub>15</sub> N <sub>1</sub> O <sub>2</sub>
Color/shape	Orange/plate
Formula weight	241.28
Temperature	296 K
Crystal system	Monoclinic
Space group	P21/c
Unit cell parameters	$a = 13.4791(11) \text{ \AA}$ $b = 6.8251(3) \text{ \AA}$ $c = 18.3561(15) \text{ \AA}$ $\alpha = 90^\circ$ $\beta = 129.296(5)^\circ$ $\gamma = 90^\circ$
Volume	1306.85(16) $\text{\AA}^3$
Z	4
Density	1.226 $\text{Mgm}^{-3}$
Absorption coefficient	0.086 $\text{mm}^{-1}$
Diffractometer/meas. meth.	STOE IPDS 2/ $\omega$ -scan
$\theta$ range for data collection	2.83–26.50°
Unique reflections measured	14,753
Total reflection/observed reflections	2704/2132
Goodness of fit on F <sup>2</sup>	1.15
Final R indices [ $I > 2\sigma(I)$ ]	$R_1 = 0.165$ , $wR_1 = 0.155$
R indices (all data)	$R_2 = 0.058$ , $wR_2 = 0.073$

Frontier molecular orbital (FMO) analysis have been used to clarify the information regarding charge transfer within the molecule. HOMO–LUMO energy gap provides important information about stability of the structure. Besides, energy gap has a major role in non-linear optic materials.

The theoretical electronic absorption spectra have been calculated by using TD-DFT method. The values of excitation energies, oscillation strengths ( $f$ ), wavelengths ( $\lambda$ ) and energy gaps of the molecule have been calculated for gas phase and different solutions. Since solvent effects play an important role in absorption spectrum of the compound, in this paper, the integral equation formalism polarizable continuum model (PCM) [26,27] dealing with solvent effect was chosen in excitation energy calculations. Solvents with different polarities, dielectric constants and protic/aprotic properties have affected the values of total energy, excitation energy,  $E_{\text{HOMO}}$ ,  $E_{\text{LUMO}}$  and dipole moment. Frontier molecular orbital (FMO) energies, energy gap ( $\Delta E$ ) and dipole moment tends to increase with increasing polarity of the solvent. Different solvents ( $\epsilon = 78.39$ , water;  $\epsilon = 46.7$ , DMSO;  $\epsilon = 24.3$ , ethanol;  $\epsilon = 4.9$ , chloroform;  $\epsilon = 2.3$ , benzene) at the B3LYP/6-31G(d,p) were carried out by using the PCM method.

The natural bonding orbitals (NBO) calculations were performed using NBO program [28] under Gaussian 03 W [30] package at the DFT/B3LYP/6-31G(d,p) level. NBO calculations interpret various second order interactions between the filled orbitals of one subsystem and vacant orbitals of another subsystem, which is a measure of the intramolecular delocalization or hyper conjugation. The redistribution of electron density in various bonding, antibonding orbitals and  $E^{(2)}$  (energy difference between donor and acceptor natural bond orbitals) energies have been calculated by natural bond orbital (NBO) analysis to give clear evidence of stabilization originating from the hyperconjugation of various intramolecular interactions.

Molecular electrostatic potential analysis (MEP) has been used to find the reactive sites of the compound. The electrostatic potential contour map with the negative regions (assigned to red) of MEP are related to electrophilic attacks and positive regions (assigned to blue) are related to nucleophilic reactivity. In addition, the net charges are calculated with Mulliken population method and natural population method (NPA). The calculated natural atomic charges values were obtained from NBO analysis.

## Results and discussion

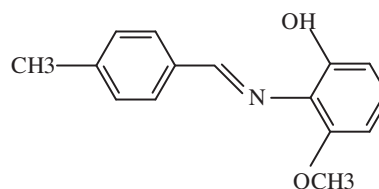
### Crystal structure and optimized geometry

The optimized molecular structure of the schiff base with atom numbering scheme adopted in this study is shown in Scheme 1. The molecule have the space group  $P21/c$ , with four molecules per unit cell ( $Z = 4$ ). From single crystal X-ray diffraction data, it is found that the crystal belongs to monoclinic which have the following dimensions;  $a = 13.4791(11)$  Å,  $b = 6.8251(3)$  Å,  $c = 18.3561(15)$  Å and the angle of  $\beta = 129.296(5)^\circ$ .

The tautomerism appears in o-hydroxy Schiff bases as a result of intramolecular proton transfer from oxygen atom to nitrogen atom. This proton transfer resulted in two tautomeric structures as enol and keto forms in the solid state. These tautomeric forms are related to two types of intramolecular hydrogen bonds as  $\text{O}=\text{H} \cdots \text{N}$  in enol form and  $\text{N}=\text{H} \cdots \text{O}$  in keto form and  $\text{N}^+=\text{H} \cdots \text{O}^-$  in zwitterionic forms. In our study of title compound is inclined to enol form because of the strong  $\text{O1}=\text{H1} \cdots \text{N1}$  intramolecular hydrogen bonding (Fig. 1, Table 2).

A significant intramolecular interaction ( $\text{O1}=\text{H1} \cdots \text{N1}$ ) is noted involving phenol atom O1 and nitrogen atom N1 and constitutes a six-membered ring  $\text{S}(6)$  [29]. The study compound has no intermolecular hydrogen bonding. The weak van der Waals interactions is also effective in crystal packing. The single bond lengths of the  $\text{C1}=\text{N1}$  (1.420(2) Å),  $\text{C8}=\text{C9}$  (1.445(2) Å),  $\text{C14}=\text{O1}$  (1.341(2) Å), and strong double bond character of the  $\text{C8}=\text{N1}$  (1.279(2) Å) are showing that this bond lengths are confirmed enol-imine tautomeric form. This characteristic bond lengths are in harmony with previous works [30,31].

X-ray results show the dihedral angle between the planes of two aromatic rings is  $23.16(6)^\circ$  and in optimized geometry it is



Scheme 1. Chemical diagram of (E)-3-methoxy-2-[(p-tolylimino)methyl]phenol.

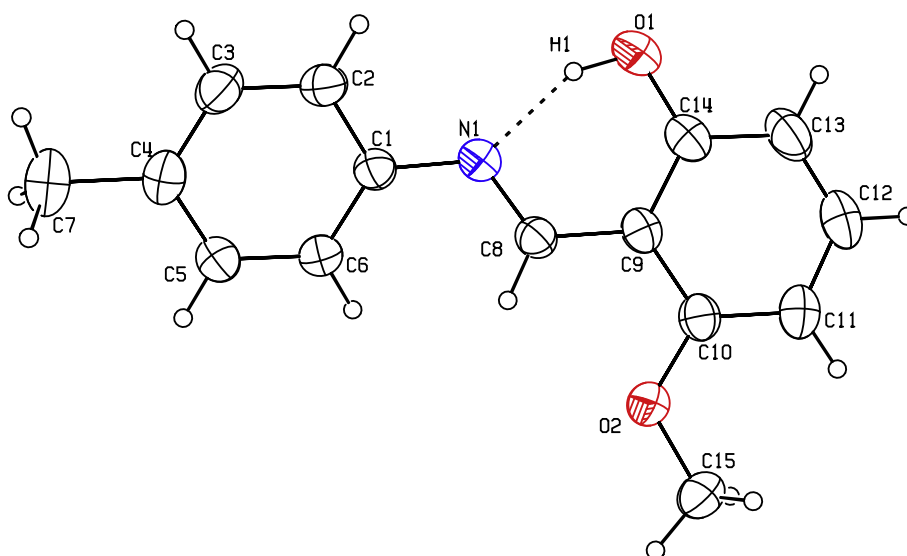


Fig. 1. Ortep 3 diagram for (E)-3-methoxy-2-[(p-tolylimino)methyl]phenol, with the atom numbering scheme. Dashed lines are show the  $\text{O1}=\text{H1} \cdots \text{N1}$  intra molecular hydrogen bonds.

**Table 2**  
Hydrogen bonding geometry for the title compound.

D—H...A	D—H	H...A	D...A	D—H...A
O1—H1...N1	0.9(3)	1.76(3)	2.59(2)	154(3)

33.84°. The nearly planar of the planes show the thermochromic properties. In addition, the dihedral angle between the nearly planar S(6) ring with C1—C6 and C9—C14 aromatic rings are 23.54(24)° and 0.38(5)°, respectively.

The optimized (theoretical) geometry parameters were calculated by B3LYP/6-31G(d,p). The selected bond lengths, bond angles and torsion angles for the optimized structure and X-ray geometry of the molecule are listed in Table 3. As expected, the results show a little difference in experimental and computational processes. The difference observed between the experimental and theoretical parameters are due to the ignored effects. These effects are the molecular interactions which the theoretical methods cannot take into account. While the experimental results belong to the solid state, the calculated results belong to the isolated gaseous phase.

Namely, the optimized geometry with B3LYP is preferred more planar conformation than X-ray geometry. The structural discrepancies between the optimized molecule and crystallographically observed geometry can be analyzed quantitatively by root mean square (r.m.s.) overlay. The r.m.s. fit of the atomic positions of experimental and calculated geometries is 0.152 Å, indicating the agreement between the two geometries (Fig. 2).

#### Vibrational spectra

Experimental and calculated FT-IR spectrum of the title compound was given in Fig. 3 and vibration frequencies of compound are compared in Table 4. The vibrational frequencies obtained by quantum chemical calculation are typically larger than their experimental counterparts, and thus, empirical scaling factors are usually used to match the experimental vibrational frequencies [32]. The computational studies on vibrational frequencies were performed at B3LYP/6-31G(d,p) level. In order to improve the

**Table 3**  
Selected molecular structure parameter for the title compound.

Bond lengths (Å), bond angles (°) and torsions (°)	Experimental	DFT/6-31G(d,p)
C1—C2	1.37(2)	1.403
C4—C7	1.51(3)	1.35
N1—C1	1.42(2)	1.40
N1—C8	1.27(2)	1.29
C8—C9	1.44(2)	1.44
O1—C14	1.48(4)	1.51
O1—H1	0.90(2)	1.00
C10—O2	1.36(2)	1.36
O2—C15	1.41(2)	1.42
C7—C4—C3	121.6(2)	121.01
C7—C4—C5	121.0(2)	121.20
C1—N1—C8	120.42(14)	121.19
N1—C8—C9	121.98(15)	121.63
C14—O1—H1	104.9(16)	107.03
C9—C8—H8	119.0	116.95
C10—O2—C15	118.56(14)	118.57
C2—C1—N1	117.63(15)	117.87
C8—H8—N1	119.0	121.40
C8—C9—C10	120.02(15)	120.48
C9—C8—N1—C1	−178.47(16)	177.29
C2—C1—N1—C8	153.98(18)	149.03
C8—C9—C10—C11	−178.83(17)	−179.98
C11—C10—O2—C15	1.6(3)	0.375
C9—C10—O2—C15	−179.54(18)	−179.74
N1—C1—C2—C3	−177.93(18)	−179.90

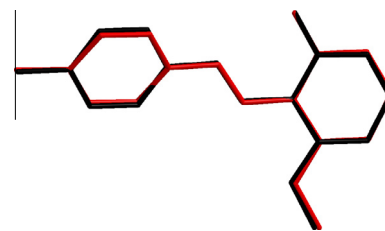


**Fig. 2.** Superimposition of the X-ray structure (red) and calculated structure (black) of the title molecule. (For interpretation of the references to color in this figure legend, the reader is referred to the web version of this article.)

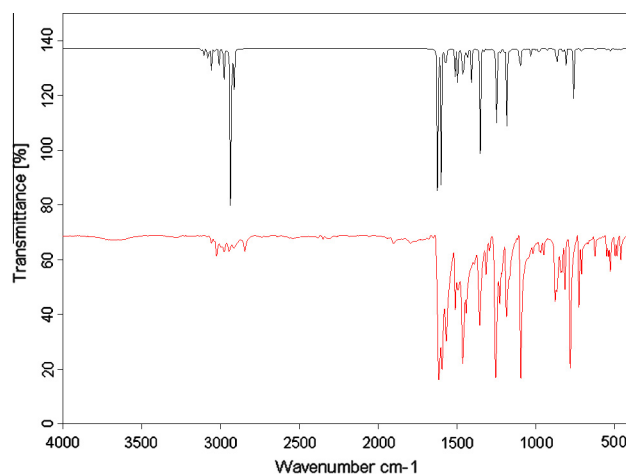


**Fig. 3.** Experimental (red) and theoretical DFT/B3LYP/631G(d,p) (black) FT-IR spectrum of the title compound. (For interpretation of the references to color in this figure legend, the reader is referred to the web version of this article.)

agreement between the calculated and the experimentally observed values, the calculated harmonic frequencies have been scaled down via introduction of scaling factor. The vibrational frequencies were scaled by 0.9627 [33]. The frequencies obtained by theoretical method is in accordance with the observed FT-IR spectrum. Theoretical and experimental FT-IR spectrum of the title molecule was given in Fig. 3.

Depending on X-ray and IR results, the title compound shows enol form rather than keto form. In the spectrum, there are two important absorption bands to characterize the title compound. One of these appears at 2000–3000 cm<sup>−1</sup> region. It is attributed to the  $\nu(\text{O1—H1})$  stretching vibration peak which broaden due to the formation of strong intramolecular O1—H1...N1 hydrogen bond in the structure. The  $\nu(\text{O1—H1})$  band is observed at 2931.8 cm<sup>−1</sup> in theoretical of FT-IR result. These stretching mode which was also supported by the literature. The result obtained from X-ray diffraction study, indicates that C8=N1 is the double bond character. As a result of this, absorption band at 1615.16 cm<sup>−1</sup> corresponds to  $\nu(\text{C8=N1})$  stretching vibration. The other characteristic IR absorption band at 3023.76–2975.86 cm<sup>−1</sup> corresponds to  $\nu(\text{C—H})$  stretching vibrations of aromatic benzene rings. The agreement between calculation results and experimental results are very good. The  $\gamma(\text{=C—H})$  rocking vibrations of aromatic structures generally occur in the region 1370–1350 cm<sup>−1</sup>. The absorption band at 1365 cm<sup>−1</sup> corresponds to  $\gamma(\text{C8—H8})$  rocking vibrations of the title compound. In addition, the experimental IR results show the aromatic  $\beta(\text{C—H})$  out-of-plane bending vibrations appear in 815.76–753.47 cm<sup>−1</sup> frequency. The rocking vibrations of  $\gamma(\text{C7—H}_3)$  group are generally observed in the region 1070–1010 cm<sup>−1</sup> [34]. This mode appears at 1017.65 cm<sup>−1</sup> and 1024.7 cm<sup>−1</sup> in experimental and theoretical FT-IR spectrum,

**Table 4**  
Comparison of the experimental and calculated vibrational frequencies ( $\text{cm}^{-1}$ ).

Experimental IR with KBr	DFT/B3LYP/631-G(d,p)	Assignments <sup>a</sup>
3023.76	3068.36 3056.35 3101.74 3115.46	$\nu(\text{C-H})$ R2 + $\nu(\text{C-H})$ R1
–	3078.44 3083.31	$\gamma(\text{C-H})$ R1
3023	3006.5	$\alpha(\text{C7-H}_3)$
2975	2978.5	
2900–3000	3005.5	$\gamma(\text{N1=C8-H8})$
2944.56	2973.7	$\nu(\text{O2-C15-H}_3)$
2844.90	2922.2	
2000–3000	2931.8	$\nu(\text{O1-H1})$
2900	2910.77	$\alpha(\text{O2-C15-H}_3)$
1463.41	1462	
1567.79	1567.14	$\nu(\text{N=C-C}) + \nu(\text{C-C})\text{R1,R2} + \gamma(\text{C-H})\text{R2}$
1597.79	1595.19 1618.2	
1615.16	1567.14	$\gamma(\text{N=C})$
1493.98	1489.29	$\nu(\text{C-C})\text{R1,R2} + \gamma(\text{C-H})\text{R1,R2} + \gamma(\text{C15-H}_3)$
1567.79	1506.6 1558.6	
1463.41	1455.6	$\nu(\text{C-C})\text{R2} + \gamma(\text{C-H})\text{R2} + \gamma(\text{O1-H1}) + \omega(\text{N=C-C})$
1441.15	1429.6	$\gamma(\text{C15-H}_3)$
1365.74	1345.85	$\gamma(\text{C8-H8})$
1228.45	1243.8	$\nu(\text{O2-C15}) + \gamma(\text{C-H})\text{R2}$
1294.02		
1186.25	1177.38	$\nu(\text{C-N}) + \gamma(\text{C-H})\text{R1,R2}$
1095.24	1093.79	$\nu(\text{O2-C15}) + \beta(\text{C-H})\text{R1,R2}$
1017.64	1024.7	$\gamma(\text{C7-H}_3)$
877.5	860.48	$\gamma(\text{O1-H1})$
841.62	862.36	
815.76	800.9	$\beta(\text{C-H})\text{R1} + \beta(\text{C-H})\text{R2}$
781.65	753.47	

<sup>a</sup>  $\nu$ , stretching;  $\gamma$ , rocking;  $\alpha$ , scissoring,  $\omega$ , wagging;  $\beta$ , bending. Abbreviations: R1, C1–C6; R2, C9–C14 phenyl ring.

respectively. The other vibrational frequencies can be seen in Table 4, particularly.

#### Frontier molecular orbitals (FMOs) and UV–vis absorption spectra

The FMOs (frontier molecular orbitals) are important in determining such properties as molecular reactivity and the ability of a molecule to absorb light. These FMOs are very important for optical and electric properties [35]. Both the highest occupied molecular orbitals (HOMOs) and lowest unoccupied molecular orbitals (LUMOs) are the main orbitals taking part in chemical stability. The HOMO represents the ability to donate an electron, LUMO as an electron acceptor representing the ability to obtain an electron.

The HOMO and LUMO energy calculated by B3LYP/6-31G(d,p) method as shown below:

$$\begin{aligned} \text{HOMO energy (B3LYP)} &= -5.57 \text{ eV} \\ \text{LUMO energy (B3LYP)} &= -1.49 \text{ eV} \\ \text{HOMO-LUMO energy gap (B3LYP)} &= 4.08 \text{ eV} \end{aligned}$$

This electronic absorption corresponds to the transition from the ground to the first excited state and is mainly described by one electron excitation from the highest occupied molecular orbital (HOMO) to the lowest unoccupied molecular orbital (LUMO). The calculations indicate that the title compound have 66 occupied molecular orbitals. Fig. 4 shows the surfaces of HOMO and LUMO and their energies. The HOMO–LUMO energy gap explains the eventual charge transfer interactions taking place within the molecule and it is also can be supported with NLO results, as we describe later. The ionization energy ( $I$ ) and electron affinity ( $A$ ) can be obtained as,  $I = -E_{\text{HOMO}}$  and  $A = -E_{\text{LUMO}}$ . Mulliken electronegativity ( $\chi$ ) can be calculated as follows:  $\chi = (I + A)/2$ . Softness ( $S$ ) is a property of molecule that measures the extent of chemical reactivity. It is the reciprocal of hardness  $S = 1/2\eta$ . It is defined as the reciprocal of hardness ( $\eta$ ) and  $\eta = (I - A)/2$  [19]. The electrophilicity index ( $\omega$ ),  $\omega = (-\chi^2/2\eta)$  is a measure of energy lowering due to maximal electron flow between donor and acceptor. The values of electronegativity, chemical hardness, softness, and electrophilicity index are 3.05 eV, 2.04 eV, 0.24 eV,  $-3.05$  eV in gas phase, respectively for the title molecule. A large HOMO–LUMO gap implies high stability. High stability of a molecule reflects its low reactivity toward chemical reactions in some sense. Considering the chemical hardness, large HOMO–LUMO gap means a hard molecule and small HOMO–LUMO gap means a soft molecule. We can assume that the stability of the molecule to softness with least HOMO–LUMO gap. In addition, soft molecules has an easily changed electron distribution so it is corresponding to more reactive site than hard molecules.

TD-DFT at B3LYP/6-31G(d,p) level by adding polarizable continuum model (PCM) calculations were started from gas phase and solution phase optimized geometry using same level of theory. As a result of theoretical calculation, excitation energies, oscillation strengths ( $f$ ), wavelengths ( $\lambda$ ), energy gaps ( $E_{\text{HOMO}} - E_{\text{LUMO}}$ ) and total energies were obtained successfully.

The UV–vis spectra of the title compound in various organic solvents (ethanol, DMSO, benzene and chloroform) were recorded within 200–800 nm range (Fig. 5). The characteristic experimental UV–vis absorption bands of the molecule in ethanol, DMSO, chloroform and benzene are comparatively given in Table 5. It is observed for all solvents that there are absorption bands less than 400 nm. The theoretical UV–vis spectrum of the title compound in several solvents (benzene, chloroform, ethanol, DMSO and water) has been studied. We give priority to these solvents because of chloroform and benzene is a nonpolar solvent, DMSO is a polar aprotic solvent. Besides, ethanol is a polar protic solvent acting as both hydrogen

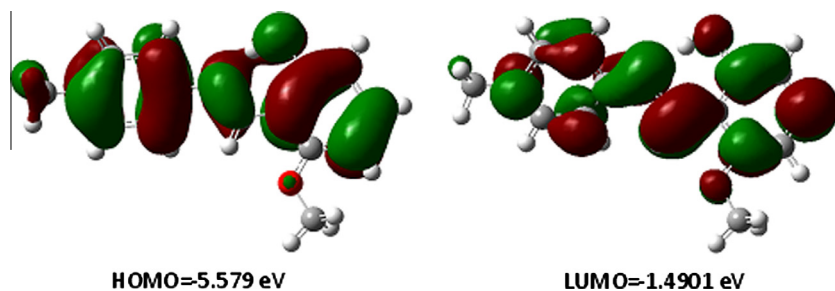
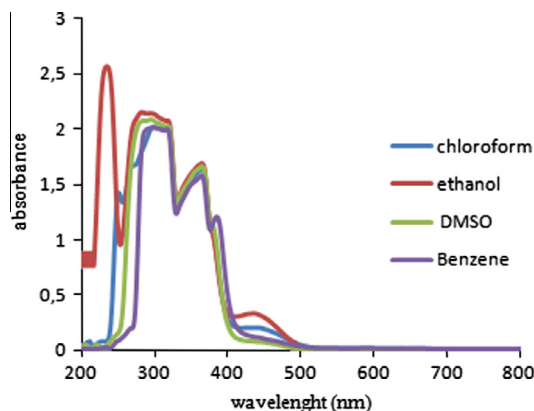


Fig. 4. Molecular orbital surfaces and energies for the HOMO and LUMO of the title compound.



**Fig. 5.** The solvent effect on UV–vis spectra of the title compound in DMSO, ethanol, chloroform and benzene.

donor and acceptor and water is not a dissolvent for the title compound. The greater the dielectric constant, the greater the polarity. These solvents cover a wide range of polarities and they have different dielectric constants (benzene  $\epsilon = 2.3$ ; chloroform  $\epsilon = 4.9$ ; EtOH  $\epsilon = 24.3$ ; DMSO  $\epsilon = 46.7$  and Water  $\epsilon = 78.39$ ).

In the UV–vis spectra of *o*-hydroxy schiff base compounds, the presence of an absorption band at less than 400 nm indicates the enol imine tautomeric form. On the other hand, compounds adopt keto-amine tautomeric form show a new absorption band at greater than 400 nm [36,37]. It is clear from our results that there is no absorption band observed at greater than 400 nm region in any solvent for the title compound. This station is supported that the molecule adopts the enol form rather than keto form. As can be seen in Table 5, the experimental wavelengths are lower than 400 nm and in the theoretical UV–vis spectrum of the title molecule absorption bands occur at 341.07 nm, 344.19 nm, 343.04 nm, 341.64 nm, 343 nm and 341.07 nm for gas phase, benzene, chloroform, ethanol, DMSO and water, respectively. The results of our analysis support that the compound show enol form rather than keto form, obviously.

In the evaluation of the results was based on the oscillator strengths ( $f$ ) which greater than 0.4. It is well known that  $\pi \rightarrow \pi^*$  transition is shifted to long wavelength with increasing the solvent polarity. The reason of this shifting, the dipole moment of solvent is produced dipole moment over the solute matter. The frontier molecular orbitals were mainly localized over the whole molecule except for methyl groups and  $\pi \rightarrow \pi^*$  interactions were common in the molecule. Then, we can say that the electronic transitions are mainly derived from the contribution of bands  $\pi \rightarrow \pi^*$  transition.

The total energy, energy gap, dipole moment, and oscillator strength increase with the increasing polarity of the solvent. Charge delocalization of the molecule increases with the increasing polarity of solvent, therefore, induces the dipole moments raised. However, excitation energies (wavelengths) were not changed linearly with increasing polarity. For why, deviations from linearity is likely related to chemical properties for solvents.

As well, FMOs are the most important orbitals because they play important roles in chemical reactions. The energy gap ( $\Delta E$ ) is important to influence the stability of a molecule and determines the chemical reactivity, kinetic stability, polarizability and chemical activity of a molecule [38]. If the molecule have a large energy gap, they are more stable molecule as a chemical activity. As a known, hard molecules have large energy gap and soft molecules have small energy gap. So, softs are more polarizable and more chemical reactive regions than hard molecules [39]. With respect to results, title compound is more polarizable, more reactive and more soft molecule as related compounds [40,41].

#### Molecular electrostatic potential

Molecular electrostatic potential (MEP) is related to the electronic density and is a very useful descriptor in understanding sites for electrophilic attack and nucleophilic reactions as well as hydrogen bonding interactions [42,43]. The electrostatic potential  $V(r)$  is also well suited for analyzing processes based on the “recognition” of one molecule by another, as in drug–receptor, and enzyme substrate interactions, because it is through their potentials that the two species first “see” each other. For the systems studied the MEP values were calculated as described previously, using the Eq. (1) [44]:

$$V(r) = \sum \frac{Z_A}{|R_A - r|} - \int \frac{\rho(r')}{|r' - r|} dr' \quad (1)$$

where the summation runs over all the nuclei  $A$  in the molecule and polarization and reorganization effects are neglected.  $Z_A$  is the charge of the nucleus  $A$ , located at  $R_A$  and  $\rho(r')$  is the electron density function of the molecule. Experimental  $V(r)$  computed with electron densities obtained from X-ray diffraction data has been used to explore the electrophilicity of hydrogen bonding functional groups. In the majority of the MEPs, while the maximum positive region which preferred site for nucleophilic attract indications as blue color, the maximum negative region which preferred site for electrophilic attract indications as red color. The different values of the electrostatic potential at the surface are represented by different colors. Potential increases in the order red < orange < yellow < green < blue. The color code of these maps is in the range between  $-0.0462$  a.u. (deepest red) and  $0.0462$  a.u. (deepest blue) in compound, where blue shows the strongest attraction and red shows the strongest repulsion. Regions of negative  $V(r)$  is usually associated with the lone pair of electronegative atoms. The study of experimental and theoretical  $V(r)$  shows that H-donor and H-acceptor properties of molecules are revealed by positive and negative regions, respectively, so that the formation of a H-bond can be regarded as the consequence of a complementarity between the electrostatic potentials [45]. According to MEP map analysis results, the negative regions of whole molecule is located on oxygen atoms (red coded region) and the positive regions (blue encoded regions) of whole molecule is located on the methyl group attached to

**Table 5**

Calculated energies, excitation energies, oscillator strengths, dipole moments and frontier orbital energies for the title compound.

	Gas phase ( $\epsilon = 1$ )	Benzene ( $\epsilon = 2.3$ )	Chloroform ( $\epsilon = 4.9$ )	Ethanol ( $\epsilon = 24.3$ )	DMSO ( $\epsilon = 46.7$ )	Water ( $\epsilon = 78.39$ )
$E_{TOTAL}$ (a.u.)	−785.8516	−785.8571	−785.8599	−785.8620	−785.8622	−785.8630
$E_{HOMO}$ (eV)	−5.57	−5.7021	−5.7443	−5.7753	−5.7813	−5.7742
$E_{LUMO}$ (eV)	−1.49	−1.5725	−1.613091	−1.64356	−1.649826	−1.6403
$\Delta E$ (eV)	4.08	4.1295	4.1312	4.1317	4.1320	4.1339
Excitation energy (nm)	341.07	344.19	343.04	341.64	343	341.07
Oscillator strength ( $f$ )	0.5086	0.5236	0.5278	0.4965	0.5821	0.4965
$\mu$ (D)	3.4166	3.8973	4.1705	4.3951	4.4129	4.4678
Experimental wavelength (nm)	–	304	298	235	296	–

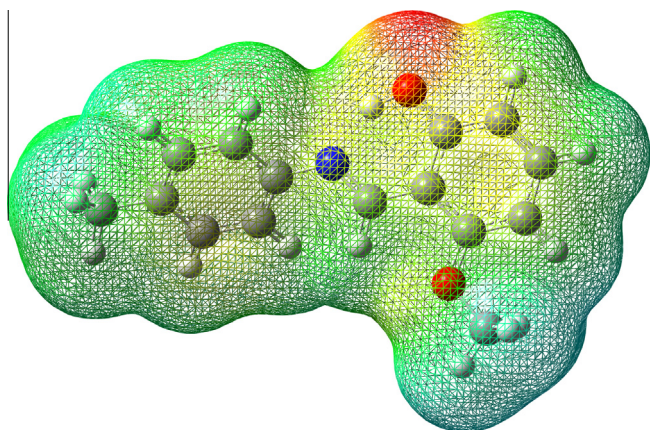


Fig. 6. Molecular electrostatic potential map calculated at B3LYP/6-31G(d,p).

the carbonyl group and concentrated on the hydrogen atoms around.

As a shown in Fig. 6, there are several possible sites for electrophilic attacks over the O1, O2 and N1 atoms. The maximum negative electrostatic potential is substantially over the O1 atom because of the strong intramolecular hydrogen bond. As can be seen from the MEP map of the title molecule, while regions having the negative potential are over the electronegative atoms, the regions having the positive potential are over the hydrogen atoms.

Red and blue regions in the MEP map refer to the regions of negative and positive potentials and correspond to the electron rich and electron-poor regions, respectively, whereas the green color signifies the neutral electrostatic potential. The MEP surface provides necessary information about the reactive sites.

#### Mulliken population analysis and natural population analysis

The calculation of effective atomic charges plays a dominant role in the application of quantum mechanical calculations to molecular systems. The Mulliken analysis is the most common population analysis method. This calculation which depicts the charges of the every atom in the molecule distribution of positive and negative charges are vital to increase or decrease of bond length between the atoms. The survey of literature reveals that effective atomic calculations gave an important role in the application of chemical calculation to molecular system because of atomic charges effect dipole moment, molecular polarizability, electronic structure, acidity–basicity behavior and a lot of properties of molecular system [46]. In addition, it also has been used to describe the electrostatic potential surfaces [47–49]. The total atomic charge values are obtained by Mulliken population analysis and natural charges are obtained by NBO (natural bond analysis) [50] are listed in Table 6. The two methods predict the same tendencies. As can be seen in Table 6, all the hydrogen atoms have a net positive charge. The obtained atomic charge shows that the H1 atom has bigger positive atomic charge (0.31 e; 0.51 e) than the other hydrogen atoms. N1, O1 and O2 atoms are most negative atomic charges (−0.61 e; −0.52 e), (−0.52 e; −0.69 e), (−0.55 e; −0.52 e). According to these results, NBO's net charges are slightly longer than Mulliken charges. The intention is to accurately model partial charge magnitude and location within a molecule. Mulliken population analysis is a good way to account for differences in electronegativities of atoms within the molecule and frequently uses for supporting the MEP contour map. MEP and Mulliken population method can be used for interpreting and predicting the reactive behavior of a wide variety of chemical systems in both electrophilic and nucleophilic reactions.

Table 6

Calculated net charges by Mulliken population method and natural population analysis (NPA).

Atom	B3LYP/6-31G (d,p) Mulliken charges	B3LYP/6-31G (d,p) (NPA) natural charges
C1	0.24	0.13
C2	−0.03	−0.22
C3	−0.09	−0.22
C4	0.08	−0.03
C5	−0.09	−0.22
C6	−0.05	−0.25
C7	−0.34	−0.69
C8	0.24	0.12
C9	−0.02	−0.23
C10	0.29	0.36
C11	−0.09	−0.36
C12	−0.04	−0.18
C13	−0.04	−0.31
C14	0.25	0.40
C15	−0.04	−0.32
N1	−0.6	−0.52
O1	−0.52	−0.69
O2	−0.55	−0.52
H1	0.31	0.51
H2	0.05	0.24
H3	0.04	0.23
H5	0.03	0.23
H6	0.05	0.24
H7A	0.12	0.24
H7B	0.12	0.24
H7C	0.10	0.24
H8	0.07	0.22
H11	0.04	0.24
H12	0.05	0.24
H13	0.05	0.25
H15A	0.11	0.20
H15B	0.11	0.20
H15C	0.11	0.23

#### Natural bond orbital (NBO) analysis

Natural bond orbital analysis provide an efficient method for studying intra and inter molecular bonding and interaction among bonds, and provides a convenient basis for investigating charge transfer or conjugative interaction in molecular systems [51]. The bonding–anti bonding interaction can be quantitatively described in terms of the NBO approach that is expressed by means of second-order perturbation interaction energy  $E^{(2)}$  [52–55]. This energy represents the estimate of the off-diagonal NBO Fock matrix element. The stabilization energy  $E^{(2)}$  associated with  $i(\text{donor}) \rightarrow j(\text{acceptor})$  delocalisation is estimated from the second-order perturbation approach as given below:

$$E^{(2)} = q_i \frac{F^2(i,j)}{\varepsilon_j - \varepsilon_i} \quad (2)$$

where  $q_i$  is the donor orbital occupancy,  $\varepsilon_i$  and  $\varepsilon_j$  are diagonal elements (orbital energies) and  $F(i, j)$  is the off-diagonal Fock matrix element. The larger the  $E^{(2)}$  value, the more intensive is the interaction between electron donors and electron acceptors, i.e. the more donating tendency from electron donors to electron acceptors and the greater the extent of conjugation of the whole system. DFT/B3LYP/6-31G (d,p) level computation is used to investigate the various second-order interactions between the filled orbitals of one subsystem and vacant orbitals of another subsystem, which is a measure of the delocalization or hyper-conjugation. Delocalization of electron density between occupied Lewis type (bond or long pair) NBO orbitals and formally unoccupied (antibonding and Rydberg) non-Lewis NBO orbitals correspond to a stabilizing donor–acceptor interaction.

In this paper, natural bond orbital method [56] at B3LYP/6-31G(d,p) level of theory using NBO program [57] under Gaussian 2003 program package. By natural bond orbital (NBO) method, the effect of substitution on the hydrogen bond strength, the charge distributions, steric effects, and electron delocalization can be also investigated. In our study, we have investigated the intramolecular interaction, rehybridization and electron delocalization within the molecule. The corresponding results have been tabulated in Table 7.

NBOs are localized electron pair orbitals for bonding pairs and lone pairs. The hybridization of the atoms and the weight of each atom in each localized electron pair bond is calculated in the idealized Lewis structure. A normal Lewis structure would not leave any antibonding orbitals, so the presence of antibonding orbitals shows deviations from normal Lewis structures. Antibonding localized orbitals are called non-Lewis NBOs. If the occupancy is not 2.0, then there are deviations from an ideal Lewis structure (Table 7). In order to study the small deviations from idealized Lewis structure, the donor–acceptor interaction approach is adopted. Strong electron delocalization in best Lewis structure will also show up as donor–acceptor interactions. Our calculation has done by examining all possible interactions between ‘filled’ (donor) Lewis-type NBOs

and ‘empty’ (acceptor) non-Lewis NBOs. Since these interactions lead to loss of occupancy from the localized NBOs of the idealized Lewis structure into the empty non-Lewis orbitals, they are referred to as ‘delocalization’ corrections to the natural Lewis structure. As a result of our study, the structure is a type of Lewis structure with% 97.06; valance-non Lewis with% 2.77 and Rydberg non-Lewis with% 0.16.

As an be seen from results, the  $\pi$ -conjugation/resonance due to  $\pi$ -electron delocalization is involved due to the  $\pi \rightarrow \pi^*$  interactions whereas, the hyperconjugative interactions due to the various types of orbital overlaps such as  $\pi \rightarrow \pi^*$ ,  $\pi^* \rightarrow \pi^*$ ,  $\pi \rightarrow \pi^*$ ,  $\pi \rightarrow \pi^*$ . However, only  $\pi \rightarrow \pi^*$  and  $n \rightarrow \pi^*$  interactions are also possible according to experimental results.

The intramolecular hyperconjugative interactions are formed by the orbital overlap between  $\pi(C-C)$  and  $\pi^*(C-C)$  bond orbitals which result in intramolecular charge transfer causing stabilization of the system. These interactions are observed as an increase in electron density (occupancy) in (C–C) anti bonding orbitals that weakens the respective bonds [58]. The occupancy at  $\pi$  bonds for (C–C) benzene ring is ( $\sim 1.63$ – $1.70$ ) and  $\pi^*$  bonds for (C–C) benzene ring is ( $\sim 0.31$ – $0.39$ ) clearly indicates strong delocalization leading to stabilization of energy in the range of 11.15–23.56 kcal/mol. In

**Table 7**

Significant donor–acceptor interactions of (E)-3-methoxy-2-[(p-tolylimino)methyl]phenol and their second order perturbation energies calculated at B3LYP level using 6-31G(d,p) basis set.

Donor(i) (occupancy)	Type	ED <sub>A</sub> ,% ED <sub>B</sub> ,%	Acceptor (j) (occupancy)	Type	ED <sub>A</sub> ,% ED <sub>B</sub> ,%	$E^{(2)}$ <sup>a</sup> (kcal/mol)	$E_j - E_i^b$ (a.u.)	$F(i, j)^c$ (a.u.)
BD C1–C2 (1.97392)	$\sigma$	50.85 49.15	RY * C3 (0.00470)	–	–	0.74	1.98	0.034
BD C1–C2 (1.97392)	$\sigma$	50.85 49.15	BD * C1–C6 (0.02963)	$\sigma^*$	49.48 50.52	3.37	1.25	0.058
BD C1–C2 (1.97392)	$\sigma$	50.85 49.15	BD * C1–N1 (0.02830)	$\sigma^*$	59.98 40.02	1.24	1.14	0.034
BD C1–C2 (1.97392)	$\sigma$	50.85 49.15	BD * C2–C3 (0.01283)	$\sigma^*$	50 50	2.46	1.28	0.050
BD C1–C2 (1.97392)	$\sigma$	50.85 49.15	BD * C8–N1 (0.01156)	$\sigma^*$	60.10 39.90	2.33	1.28	0.049
BD C2–C3 (1.68664)	$\pi$	49.79 50.21	BD * C1–C6 (0.39055)	$\pi^*$	50.40 49.60	19.73	0.28	0.068
BD C2–C3 (1.68664)	$\pi$	49.79 50.21	BD * C4–C5 (0.34993)	$\pi^*$	50.61 49.39	19.93	0.29	0.068
BD C1–C6 (1.63850)	$\pi$	49.60 50.40	BD * C4–C5 (0.34993)	$\pi^*$	50.61 49.39	20.28	0.29	0.068
BD C1–C6 (1.63850)	$\pi$	49.60 50.40	BD * C2–C3 (0.31653)	$\pi^*$	50.21 49.79	18.67	0.29	0.066
BD C1–N1 (1.98351)	$\sigma$	40.02 59.98	BD * C8–C9 (0.02466)	$\sigma^*$	51.52 48.48	3.14	1.28	0.057
BD C1–N1 (1.98351)	$\sigma$	40.02 59.98	BD * C8–N1 (0.01156)	$\sigma^*$	60.10 39.90	1.60	1.37	0.042
BD C1–N1 (1.98351)	$\sigma$	40.02 59.98	BD * O1–H1 (0.08761)	$\sigma^*$	20.35 79.65	0.52	1.21	0.023
BD C4–C5 (1.64608)	$\pi$	49.39 50.61	BD * C1–C6 (0.39055)	$\pi^*$	50.40 49.60	20.90	0.28	0.068
BD C4–C7 (1.98423)	$\sigma$	50.71 49.29	BD * C4–C5 (0.02249)	$\sigma^*$	49.46 50.54	1.97	1.20	0.043
BD C8–C9 (1.97429)	$\sigma$	48.48 51.52	BD * C1–N1 (0.02830)	$\sigma^*$	59.98 40.02	4.20	1.13	0.062
BD C8–C9 (1.97429)	$\sigma$	48.48 51.52	BD * C8–N1 (0.01156)	$\sigma^*$	60.10 39.90	1.80	1.28	0.043
BD C8–C9 (1.97429)	$\sigma$	48.48 51.52	BD * C9–C14 (0.03440)	$\sigma^*$	48.55 51.45	2.66	1.21	0.051
BD C8–N1 (1.98708)	$\sigma$	39.90 60.10	BD * O1–H1 (0.08761)	$\pi^*$	20.35 79.65	1.76	1.31	0.044
BD C8–N1 (1.98708)	$\sigma$	39.90 60.10	RY * C9 (0.00635)	–	–	2.09	2.20	0.061
BD C8–N1 (1.91160)	$\pi$	37.54 62.46	BD * C1–C6 (0.39055)	$\pi^*$	50.40 49.60	11.15	0.36	0.062
BD C9–C10 (1.96813)	$\sigma$	50.80 49.20	BD * C14–O1 (0.01760)	$\sigma^*$	66.13 33.87	3.24	1.10	0.054
BD C9–C10 (1.96813)	$\sigma$	50.80 49.20	BD * C15–O2 (0.00828)	$\sigma^*$	68.38 31.62	2.92	0.97	0.048

(continued on next page)

Table 7 (continued)

Donor(i) (occupancy)	Type	ED <sub>A</sub> ,% ED <sub>B</sub> ,%	Acceptor (j) (occupancy)	Type	ED <sub>A</sub> ,% ED <sub>B</sub> ,%	E <sup>(2)</sup> <sup>a</sup> (kcal/mol)	E <sub>j</sub> – E <sub>i</sub> <sup>b</sup> (a.u.)	F(i, j) <sup>c</sup> (a.u.)
BD C9–C10 (1.96813)	σ	50.80 49.20	BD * C10–C11 (0.02486)	σ*	49.54 50.46	3.39	1.26	0.058
BD C9–C14 (1.97360)	σ	51.45 48.55	BD * C10–O2 (0.02782)	σ*	67.63 32.37	3.10	1.05	0.051
BD C10–C11 (1.70357)	π	43.53 56.47	LP C9 (1.14923)	–	–	32.19	0.15	0.081
BD C10–C11 (1.70357)	π	43.53 56.47	BD * C12–C13 (0.31907)	π*	54.54 45.46	23.56	0.30	0.075
BD C10–O2 (1.99133)	σ	32.37 67.63	BD * C11–C12 (0.01495)	σ*	49.56 50.44	1.07	1.48	0.036
BD C12–C13 (1.71811)	π	45.46 54.54	LP * C14 (0.90741)	–	–	57.05	0.14	0.096
BD C12–C13 (1.71811)	π	45.46 54.54	BD * C10–C11 (0.38199)	π*	56.47 43.53	13.81	0.27	0.056
BD C13–C14 (1.97794)	σ	49.45 50.55	RY * C12 (0.00483)	–	–	0.66	1.98	0.032
BD C13–C14 (1.97794)	σ	49.45 50.55	RY * C12 (0.00297)	–	–	1.60	1.40	0.042
BD C13–C14 (1.97794)	σ	49.45 50.55	RY * O1 (0.00152)	–	–	0.66	1.94	0.032
BD C13–C14 (1.97794)	σ	49.45 50.55	BD * O1–H1 (0.08761)	σ*	20.35 79.65	1.95	1.13	0.043
BD C14–O1 (1.99442)	σ	33.87 66.13	BD * C9–C10 (0.02677)	σ*	49.20 50.80	1.53	1.45	0.032
BD C15–O2 (1.99286)	σ	31.62 68.38	RY * C10 (0.00746)	–	–	1.10	1.83	0.040
BD C15–O2 (1.99286)	σ	31.62 68.38	BD * C9–C10 (0.02677)	σ*	49.20 50.80	2.81	1.37	0.056
BD O1–H1 (1.98471)	σ	79.65 20.35	BD * C13–C14 (0.02409)	σ*	50.55 49.45	5.51	1.29	0.075
LP C9 (1.14923)	–	–	BD * C8–N1 (0.21779)	π*	62.46 37.54	70.56	0.13	0.103
LP C9 (1.14923)	–	–	BD * C10–C11 (0.38199)	π*	56.47 43.53	79.57	0.14	0.108
LP C14 (0.90741)	–	–	BD * C12–C13 (0.31907)	π*	54.54 45.46	50.85	0.15	0.099
LP N1 (1.84249)	–	–	BD * O1–H1 (0.08761)	σ*	20.35 79.65	36.01	0.79	0.153

<sup>a</sup> E<sup>(2)</sup> means energy of hyperconjugative interactions (stabilization energy).

<sup>b</sup> Energy difference between donor (i) and acceptor (j) NBO orbitals.

this paper,  $n \rightarrow \pi^*$  interactions are due to the carbon lone pair electron donation from  $n(\text{C9})$  atom to (anti bonding acceptor)  $\pi^*(\text{C8}=\text{N1})$  and  $\pi^*(\text{C10}=\text{C11})$  show the strongest stabilization to the system by 70.56 kcal/mol and 79.57 kcal/mol, respectively. Besides, this interactions are strengthens the intramolecular  $\text{O1} \cdots \text{N1}$  hydrogen bond. The most important interaction energy (the most strongest energy) is related to the resonance in the title molecule and it is electron donating from lone pair ( $n$ ) and anti bonding unoccupied non-Lewis NBO orbital. The strong stabilization denotes the larger delocalization. According to our calculations, all  $\sigma \rightarrow \sigma^*$  interactions demonstrate the weak E<sup>(2)</sup> values in the range of 1.07–4.20 kcal/mol. The delocalization of electron density (occupancy) between occupied Lewis type  $\sigma(\text{C}=\text{C})$  and  $\sigma(\text{C}=\text{N})$  bonds and unoccupied antibonding Rydberg non-Lewis orbitals correspond to weak hyperconjugative interactions. In this paper, we observed  $\sigma \rightarrow \sigma^*$  interactions only in theoretical computations and these are correspond to lower E<sup>(2)</sup> values. The experimental results show  $\pi^* \rightarrow \pi^*$  and  $n \rightarrow \pi^*$  interactions, clearly. In Table 7, the% valence hybrids are also shown. In addition, hyperconjugative interactions are associated with% ED (occupancy). In order to determine the ideal Lewis type, we should check out% valence hybrids of the atoms and the weight of each atom in each localized electron pair bond.

#### Nonlinear optical effects (NLO)

Molecule-based second-order nonlinear optical (NLO) materials have recently attracted much interest because they involve new scientific phenomena and because they offer potential applications in emerging optoelectronic technologies. Molecular materials with

nonlinear optical (NLO) properties are currently attracting considerable attention because of their potential applications in optoelectronic devices of telecommunications, information storage, optical switching, and signal processing. Comparing with organic molecules, metal complexes can offer great scope for the creation of multifunctional NLO materials. Recently, various multidimensional NLO metal complexes have emerged as candidates for second-order NLO materials because of their potential advantages over one-dimensional chromophores, such as increasing  $\beta$  responses without undesirable losses of transparency in the visible region, possessed better phase-matching because of their larger off-diagonal components [59].

The output from GAUSSIAN03W provides 10 components of the  $3 \times 3 \times 3$  matrix as  $\beta_{xxx}$ ;  $\beta_{xxy}$ ;  $\beta_{xyy}$ ;  $\beta_{yyy}$ ;  $\beta_{xxz}$ ;  $\beta_{xyz}$ ;  $\beta_{yyz}$ ;  $\beta_{zzz}$ ; respectively, from which the  $x$ ;  $y$  and  $z$  components of  $\beta$  are calculated as described earlier [60]. When reporting a single value of  $\beta$ ; one of the common formats is to simply treat the three independent values for  $\beta$  as a quasi Pythagorean problem and solve for the average  $\beta$  by the following equation:

$$\beta_{\text{top}} = \sqrt{\beta_x^2 + \beta_y^2 + \beta_z^2} \quad (3)$$

The total static dipole moment  $\mu$ , the average linear polarizability  $\alpha$ , and the first hyperpolarizability  $\beta$  can be calculated by using Eqs. (4)–(6), respectively.

$$\mu = (\mu_x^2 + \mu_y^2 + \mu_z^2)^{1/2} \quad (4)$$

**Table 8**

Calculated dipole moments ( $\mu$ ), polarizability ( $\alpha$ ) and first hyperpolarizability ( $\beta$ ) components for the title compound.

$\mu_x = -0.18$ a.u.	$\beta_{xxx} = -628.51$ a.u.
$\mu_y = 1.32$ a.u.	$\beta_{xxy} = 118.33$ a.u.
$\mu_z = 0.09$ a.u.	$\beta_{xyy} = 12.364$ a.u.
$\mu_{\text{tot}} = 1.33$ Debye	$\beta_{yyy} = -25.61$ a.u.
$\alpha_{xx} = 330.36$ a.u.	$\beta_{xxz} = 80.76$ a.u.
$\alpha_{xy} = 6.37$ a.u.	$\beta_{xyz} = -16.50$ a.u.
$\alpha_{yy} = 178.90$ a.u.	$\beta_{yyz} = -9.18$ a.u.
$\alpha_{xz} = 4.34$ a.u.	$\beta_{zzz} = 7.44$ a.u.
$\alpha_{yz} = -10.84$ a.u.	$\beta_{yzz} = 15.06$ a.u.
$\alpha_{zz} = 81.20$ a.u.	$\beta_{zzz} = 7.64$ a.u.
$\alpha_{\text{tot}} = 29.16 \text{ \AA}^3$	$\beta_{\text{tot}} = 5.432 \times 10^{-30} \text{ cm}^5/\text{esu}$

$$a = \frac{1}{3}(\alpha_{xx} + \alpha_{yy} + \alpha_{zz})^2 \quad (5)$$

$$\beta_{\text{tot}} = \left[ (\beta_{xxx} + \beta_{xxy} + \beta_{xxz})^2 + (\beta_{yyy} + \beta_{yyz} + \beta_{yxx})^2 + (\beta_{zzz} + \beta_{zxx} + \beta_{zyy})^2 \right]^{1/2} \quad (6)$$

The dipole moment, polarizability and the first hyperpolarizability were calculated using polar=ENONLY at the level of B3LYP/6-31G(d,p) and the results obtained from calculation. The calculated polarizability  $\alpha$  and first hyperpolarizability  $\beta$  of title compound are  $29.16 \text{ \AA}^3$  and  $5.432 \times 10^{-30} \text{ cm}^5/\text{esu}$  and the title molecule is 14.5 times greater than those of urea ( $\alpha$  and  $\beta$  of urea of  $3.8312 \text{ \AA}^3$  and  $0.37289 \times 10^{-30} \text{ cm}^5/\text{esu}$ ), respectively [61].

The polar properties of the title molecule were calculated at the B3LYP/6-31G(d,p) level using the Gaussian 03 W program package. The calculated values of electronic dipole moment,  $\mu$ , polarizability,  $\alpha$ , and the first hyperpolarizability,  $\beta$  for the title compound are, 1.33 Debye,  $29.16 \text{ \AA}^3$ ,  $5.43 \times 10^{-30} \text{ cm}^5/\text{esu}$ , respectively (Table 8). It is well known that the substituents influence the polarity of the molecules. The energy gap between HOMO and LUMO of the title compound is 4.08 eV for gas phase. These small HOMO–LUMO energy gap for the title compound indicate that molecular charge transfer occur in the compound. Energy gap is small and it is easy to notice that they can be sensitive to the influence of the polar environment. Determination of the energy gap, the dipole moment and first order hyperpolarizability shows that the title molecule is an attractive object for future studies of non-linear optical properties.

## Conclusion

In the present work, the compound is experimentally investigated by means of X-ray diffraction, FT-IR and UV–vis spectroscopic techniques. It is concluded on the basis of X-ray and FT-IR investigations that the title compound exists in enol form in the solid state. All theoretical calculations is performed with DFT/B3LYP/6-31G(d,p). The theoretically calculated values of both bond lengths and bond angles of the structure of the minimum energy were then compared with X-ray crystallographic data. The vibrational frequencies of the fundamental modes of the compound have been precisely assigned, analyzed and the theoretical results were compared with the experimental vibrations. The net charge distribution of title compound was calculated by the Mulliken population method and natural population analysis with B3LYP/6-31G(d,p) basis set. The MEP map contour shows that the negative potential sites are on electronegative atoms as well as the positive potential sites are around the hydrogen atoms. The electronic absorption spectrum was calculated by TD-DFT method. In order to understand electronic transitions of compound, TD-DFT calculations on electronic absorption spectra in several solvents and gas

phase were performed. Computational and experimental UV–vis studies for various organic solvents of different polarities indicate that the stability of the molecule increases upon an increase in the polarity of solvent. Molecular orbital coefficient analyses suggest that the electronic spectrum corresponds to strong  $\pi \rightarrow \pi^*$  transitions. The results show that molecule exists enol form even in solvent media. The movement of  $\pi$ -electron cloud from donor to acceptor i.e. intramolecular charge transfer can make the molecule more polarized and the low HOMO–LUMO energy gap could be responsible for the non-linear optical properties of the molecule. The title compound exhibited good NLO property and it was approximately 14.5 times greater than urea. We can conclude that the title molecule is an attractive object for future studies of non-linear optical properties. Natural bond orbital (NBO) calculations reveals the delocalization or hyper-conjugation interaction, intramolecular charge transfer and stabilization energy of molecule. According to NBO results, we can determine the ideal Lewis type structure. We hope the results of this study will help researchers to analyze and synthesize new materials.

## Supplementary data

CCDC 965353 contains the supplementary crystallographic data for this paper. These data can be obtained free of charge via [www.ccdc.cam.ac.uk/data\\_request/cif](http://www.ccdc.cam.ac.uk/data_request/cif), by emailing [data\\_request@ccdc.cam.ac.uk](mailto:data_request@ccdc.cam.ac.uk), or by contacting The Cambridge Crystallographic Data Centre, 12, Union Road, Cambridge CB2 1EZ, UK; fax: +44 1223 336033.

## Acknowledgement

The authors wish to acknowledge the Faculty of Arts and Sciences, Ondokuz Mayıs University, Turkey, for the use of the STOE IPDS 2 diffractometer (purchased under Grant F.279 of the University Research Fund).

## References

- [1] R. Lozier, R.A. Bogomolni, W. Stoekenius, *Biophys. J.* 15 (1975) 955–962.
- [2] A.D. Garnovskii, A.L. Nivorozhkin, V.I. Minkin, *Coord. Chem. Rev.* 126 (1993) 1–69.
- [3] M.D. Cohen, G.M.J. Schmidt, S. Flavian, *J. Chem. Soc.* (1964) 2041–2051.
- [4] E. Hadjoudis, M. Vitterakis, I. Moustakali, I. Mavridis, *Tetrahedron* 43 (1987) 1345–1360.
- [5] I. Moustakali-Mavridis, E. Hadjoudis, A. Mavridis, *Acta Cryst. B34* (1978) 3709–3715.
- [6] E. Hadjoudis, M. Vitterakis, I. Moustakali-Mavridis, *Tetrahedron* 43 (1987) 1345–1360.
- [7] J. Costamagna, J. Vargas, R. Latorre, A. Alvarado, G. Mena, *Coord. Chem. Rev.* 119 (1992) 67–88.
- [8] V. Sridharan, S. Muthusubramanian, S. Sivasubramanian, K. Polborn, *J. Mol. Struct.* 707 (2004) 161–167.
- [9] P. Fita, E. Luzina, T. Dziembowska, D. Kopec, P. Piatkowski, Cz. Radzewicz, A. Grabowska, *Chem. Phys. Lett.* 416 (2005) 305–310.
- [10] A.P. Alivisatos, P.F. Barbara, A.W. Castleman, J. Chang, D.A. Dixon, M.L. Klein, G.L. McLendon, J.S. Miller, M.A. Ratner, P.J. Rossky, S.I. Stupp, M.E. Thompson, *Adv. Mater.* 16 (1998) 1297–1336.
- [11] L. Dalton, *Adv. Polym. Sci.* 158 (2002) 1–86.
- [12] R.E. Stratmann, G.E. Scuseria, M.J. Frisch, *J. Chem. Phys.* 109 (1998) 8218.
- [13] R. Bauernschmitt, R. Ahlrichs, *Chem. Phys. Lett.* 256 (1996) 454.
- [14] M.E. Casida, C. Jamorski, K.C. Casida, D.R. Salahub, *J. Chem. Phys.* 108 (1998) 4439.
- [15] G.M. Sheldrick, SHELXS-97. Program for the Solution of Crystal Structures, University of Göttingen, 1997.
- [16] G.M. Sheldrick, SHELXL-97. Program for Crystal Structures Refinement, University of Göttingen, 1997.
- [17] L.J. Farrugia, *J. Appl. Crystallogr.* 30 (1999) 837.
- [18] Stoe & Cie, X-AREA (Version 1.18) and X-RED32 (Version 1.04) Stoe & Cie, Darmstadt, 2002.
- [19] A.L. Spek, *Acta Crystallogr. D* 65 (2009) 148.
- [20] M.J. Frisch, G.W. Trucks, H.B. Schlegel, G.E. Scuseria, M.A. Robb, J.R. Cheeseman, J.A. Montgomery, T.J. Vreven, K.N. Kudin, J.C. Burant, J.M. Millam, S.S. Iyengar, J. Tomasi, V. Barone, B. Mennucci, M. Cossi, G. Scalmani, N. Rega, G.A. Petersson, H. Nakatsuji, M. Hada, M. Ehara, K. Toyota, R. Fukuda, J. Hasegawa, M. Ishida, T.

- Nakajima, Y. Honda, O. Kitao, H. Nakai, M. Klene, X. Li, J.E. Knox, H.P. Hratchian, J.B. Cross, C. Adamo, J. Jaramillo, R. Gomperts, R.E. Stratmann, O. Yazyev, A.J. Austin, R. Cammi, C. Pomelli, J.W. Ochterski, P.Y. Ayala, K. Morokuma, G.A. Voth, P. Salvador, J.J. Dannenberg, V.G. Zakrzewski, S. Dapprich, A.D. Daniels, M.C. Strain, O. Farkas, D.K. Malick, A.D. Rabuck, K. Raghavachari, J.B. Foresman, J.V. Ortiz, Q. Cui, A.G. Baboul, S. Clifford, J. Cioslowski, B.B. Stefanov, G. Liu, A. Liashenko, P. Piskorz, I. Komaromi, R.L. Martin, D.J. Fox, T. Keith, M.A. Al-Laham, C.Y. Peng, A. Nanayakkara, M. Challacombe, P.M.W. Gill, B. Johnson, W. Chen, M.W. Wong, C. Gonzalez, J.A. Pople, GAUSSIAN 03, Revision E.01, Gaussian Inc, Wallingford CT, 2004.
- [21] H.B. Schlegel, *J. Comput. Chem.* 3 (1982) 214–218.
- [22] P. Hohenberg, W. Kohn, *Phys. Rev.* 136 (1964) B864–B871.
- [23] A.D. Becker, *J. Chem. Phys.* 98 (1993) 5648–5652.
- [24] C. Lee, W. Yang, R.G. Parr, *Phys. Rev. B* 37 (1988) 785–789.
- [25] A. Frisch, A.B. Nielson, A.J. Holder, *Gauss View User Manual*, Gaussian Inc, Pittsburgh, PA, 2000.
- [26] S. Miertus, E. Scrocco, J. Tomasi, *Chem. Phys.* 55 (1981) 117–129.
- [27] M. Cossi, N. Rega, G. Scalmani, V. Barone, *J. Comput. Chem.* 24 (2003) 669–681.
- [28] E.D. Glendening, A.E. Reed, J.E. Carpenter, F. Weinhold, NBO version 3.1, TCI, University of Wisconsin, Madison, 1998.
- [29] J. Bernstein, R.E. Davis, L. Shimoni, N.L. Chang, *Angew. Chem. Int. Ed. Engl.* 34 (1995) 1555–1573.
- [30] M. Kabak, A. Elmali, Y. Elerman, *J. Mol. Struct.* 477 (1999) 151–158.
- [31] H. Ünver, A. Karakas, A. Elmali, *J. Mol. Struct.* 702 (2004) 49–54.
- [32] F. Jensen, *Introduction to Computational Chemistry*, Wiley, New York, 1999.
- [33] J.P. Merrick, D. Moran, L. Radom, *J. Phys. Chem. A* 111 (2007) 11683–11700.
- [34] R.M. Silverstein, G.C. Basseler, C. Morill, *Spectroscopic Identification of Organic Compounds*, Wiley, New York, 1981.
- [35] I. Fleming, *Frontier Orbitals and Organic Chemical Reactions*, Wiley, London, 1976.
- [36] H. Nazır, M. Yıldız, H. Yılmaz, M.N. Tahir, D. Ulku, *J. Mol. Struct.* 524 (2000) 241–250.
- [37] K. Ogawa, J. Harada, *J. Mol. Struct.* 647 (2003) 211–216.
- [38] H. Tanak, *J. Mol. Struct. (Theochem)* 950 (2010) 5–12.
- [39] R.G. Pearson, *Proc. Natl. Acad. Sci.* 83 (1986) 8440.
- [40] G.D. Tanga, J.Y. Zhao, R.Q. Lia, Y. Caob, Z.C. Zhanga, *Spectrochim. Acta Part A* 78 (2011) 449–457.
- [41] Y. Suna, Z. Liub, C. Yub, C. Huang, Q. Haoc, L. Xu, *Org Electron* 14 (2013) 1538–1550.
- [42] E. Scrocco, J. Tomasi, *Adv. Quantum Chem.* 11 (1978) 115–121.
- [43] F.J. Luque, J.M. Lopez, M. Orozco, *Theor. Chem. Acc* 103 (2000) 343–345.
- [44] P. Politzer, P.R. Laurence, K. Jayasuriya, *Special Issue Environ. Environ. Health Perspect.* 61 (1985) 191–202.
- [45] S.J. Grabowski, J. Leszczynski, Unrevealing the Nature of Hydrogen Bonds:  $\pi$ -electron delocalization shapes H-bond features, chapter. In: *Hydrogen Bonding-New Insights*, Academic Publishers, 2006.
- [46] I. Sidir, Y.G. Sidir, M. Kumalar, E. Tasal, *J. Mol. Struct.* 964 (2010) 134–138.
- [47] V. Balachandran, K. Parimala, *Spectrochim. Acta A* 96 (2012) 340–351.
- [48] A. Lakshmi, V. Balachandran, *J. Mol. Struct.* 1033 (2013) 40–50.
- [49] S. Ramalingama, M. Karabacak, S. Perianady, N. Puviarasan, D. Tanuja, *Spectrochim. Acta A* 96 (2012) 207–212.
- [50] R.S. Mulliken, *J. Chem. Phys.* 23 (1955) 1833–1840.
- [51] S. Muthu, J.U. Maheswari, *Spectrochim. Acta* 92A (2012) 154.
- [52] A.E. Reed, F. Weinhold, *J. Chem. Phys.* 83 (1985) 1736.
- [53] A.E. Reed, R.B. Weinhold, F. Weinhold, *J. Chem. Phys.* 83 (1985) 735.
- [54] A.E. Reed, F. Weinhold, *J. Chem. Phys.* 78 (1983) 4066.
- [55] J.P. Foster, F. Weinhold, *J. Am. Chem. Soc.* 102 (1980) 7211.
- [56] A.E. Reed, L.A. Curtiss, F. Weinhold, *Chem. Rev.* 88 (1988) 899.
- [57] E.D. Glendening, A.E. Reed, J.E. Carpenter, F. Weinhold, NBO 3.1, Theoretical Chemistry Institute, University of Wisconsin, Madison, 1996.
- [58] N. Choudhary, S. Bee, A. Gupta, P. Tandon, *Comput. Theor. Chem.* 1016 (2013) 8–21.
- [59] B.J. Coe, J.A. Harris, L.A. Jones, B.S. Brunshwig, K. Song, K. Clays, J. Garin, J. Orduna, S.J. Coles, M.B. Hursthouse, *J. Am. Chem. Soc.* 127 (2005) 4845–4859.
- [60] H. Karaer, I.E. Gümrükçüoğlu, *Turk. J. Chem. Cryst.* 23 (1999) 61.
- [61] Y.X. Sun, Q.L. Hao, W.X. Wei, Z.X. Yu, L.D. Lu, X. Wang, Y.S. Wang, *J. Mol. Struct. (Theochem)* 904 (2009) 74–82.